れの化合物も Aβ凝集体に対し高い結合親和性を示した。一方、インドール骨格の 1 位にフェニル基を導入した 1-PI 誘導体である化合物 **19** は、Ki 値が 10000 以上となり Aβ凝集体に対しらかになった。

て顕著な結合性を持たないことが示された。以上の結果より、Aβ(1-42)との結合親和性にはインドール骨格へのフェニル基の導入位置が重要であることが明

Table 1. Inhibition constants (K_i) for binding of PI derivatives determined using [^{125}I]IMPY as the ligand in Aβ (1-42) aggregates.

Compound	K_i (nM)[a]
5	27.0 ± 0.18
8	4.24 ± 0.71
11	20.2 ± 5.15
12	32.9 ± 2.93
13	25.9 ± 5.13
19	>10000

[a]Values are means ± standard error for the mean for 3-6 independent experiments.

Ⅱ-iv Tg257

6 トランスジェニックマウス脳切片を用いた蛍光染色

化合物 **8** を用いて、Tg2576 トランスジェニックマウス脳切片の蛍光染色を行い、2-PI のアミロイド斑への結合性を確認した。また、蛍光染色を用いた切片の隣接切片を用いて、老人斑アミロイド蛍光染色試薬として知られているチオフラビンSによる蛍光染色を行い、アミロイド斑の存在を確認らかになった。

した。比較として、wild-type マウス脳切片を用いた蛍光染色も行った。その結果、Tg2576 マウス脳切片上には wild-type マウス脳切片上には認められない複数の蛍光像が観察され、その蛍光像は、チオフラビン S の蛍光像と一致した。この結果より、2-PI 誘導体である化合物 **8** がマウス脳内に蓄積したアミロイド斑に対して選択的結合性を有することが明

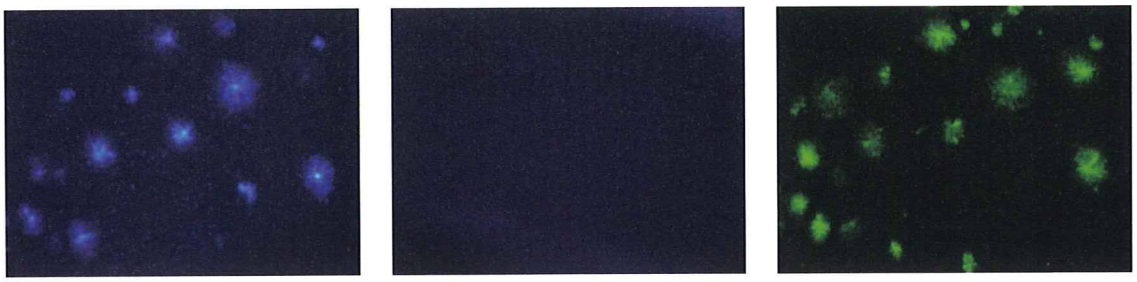

Figure 4. Neuropathological staining of compound **8** on 10-μm AD model mouse sections (left) and wild-type mouse sections (middle). Labeled plaques were confirmed by staining of the adjacent sections with thioflavin S (right).

Ⅱ－v　正常マウスを用いた体内放射能分布実験

Aβ凝集体に対して高い結合親和性を示した 2-PI 誘導体[^{125}I]**5**、[^{125}I]**8**、[^{125}I]**11**、[^{125}I]**13** に関して、正常マウスを用いた体内放射能分布実験を行った。 [^{125}I]**5**、[^{125}I]**8**、[^{125}I]**11**、[^{125}I]**13** を正常マウスに投与後の体内放射能分布の結果を Table 2 に、脳における放射能挙動を Figure 4 に示す。

[^{125}I]**5**、[^{125}I]**8**、[^{125}I]**11**、[^{125}I]**13** は、投与 2-10 分後にそれぞれ、1.7、1.2、2.1、2.6 %ID/g の放射能が脳へ移行した。しかしながら、2 分に対する 30 分の放射能の割合は、もっとも速やかなクリアランスを示した[^{125}I]**11** で 64.4%と、いずれの化合物においても脳内における滞留傾向を示した。この脳内放射能挙動の結果は、これまでに報告されたチオフラビン-T 類縁化合物の放射性ヨウ素標識体と類似したものであった。

また、2-PI にジメチルアミノ基を導入した[^{125}I]**8** は胃への著しい放射能集積が見られ、体内における不安定性が示唆される結果となった。

Table 2. Biodistribution of radioactivity after injection of [^{125}I]2-PI derivatives in normal mice[a].

Tissue	Time after injection (min)			
	2	10	30	60
		[^{125}I]**5**		
Blood	3.77 (1.25)	1.71 (0.15)	1.36 (0.15)	0.85 (0.15)
Liver	22.85 (9.60)	26.83 (1.28)	23.07 (2.33)	18.59 (5.60)

Kidney	5.53 (1.77)	4.31 (0.44)	3.84 (0.67)	2.95 (0.87)
Intestine	0.97 (0.33)	3.57 (0.34)	8.54 (1.80)	10.46 (1.11)
Spleen	7.83 (2.24)	19.67 (8.82)	10.34 (1.26)	7.77 (0.50)
Pancreas	2.31 (0.70)	2.87 (0.33)	2.12 (0.32)	1.38 (0.16)
Heart	5.68 (1.27)	3.59 (0.29)	2.96 (0.42)	2.11 (0.57)
Stomach[b]	0.52 (0.03)	1.34 (0.53)	2.55 (2.12)	1.90 (0.52)
Brain	1.10 (0.27)	1.68 (0.13)	1.42 (0.03)	0.90 (0.15)
		[^{125}I]**8**		
Blood	6.18 (0.65)	4.53 (0.37)	3.68 (0.41)	3.29 (1.00)
Liver	10.20 (1.92)	5.14 (1.01)	3.55 (0.62)	3.24 (0.76)
Kidney	9.49 (1.61)	4.46 (0.71)	4.58 (1.24)	4.71 (2.44)
Intestine	1.80 (0.24)	3.09 (0.40)	4.52 (0.58)	6.08 (1.58)
Spleen	4.13 (0.64)	3.28 (0.57)	2.60 (0.41)	2.24 (0.64)
Pancreas	5.21 (2.50)	4.13 (0.67)	3.10 (0.41)	2.30 (0.54)
Heart	8.08 (1.59)	4.82 (0.67)	1.87 (0.21)	1.84 (0.76)
Stomach[b]	4.03 (0.65)	10.65 (2.18)	17.77 (2.04)	16.26 (3.52)
Brain	1.19 (0.34)	1.19 (0.30)	0.96 (0.17)	0.71 (0.19)
		[^{125}I]**11**		
Blood	3.59 (1.41)	1.97 (0.54)	1.38 (0.25)	0.80 (0.43)
Liver	17.81 (5.73)	13.96 (4.21)	10.38 (2.64)	8.26 (2.29)
Kidney	8.76 (2.19)	4.96 (1.44)	2.89 (0.44)	2.06 (0.66)
Intestine	1.90 (0.66)	6.85 (1.86)	12.32 (3.65)	21.11 (6.94)
Spleen	4.22 (0.78)	3.43 (1.15)	2.96 (0.41)	2.04 (1.12)
Pancreas	4.54 (0.44)	3.94 (1.46)	1.95 (0.33)	1.29 (0.45)
Heart	7.72 (1.94)	2.97 (1.26)	1.47 (0.20)	1.12 (0.48)
Stomach[b]	0.72 (0.39)	1.38 (1.42)	2.67 (3.24)	3.06 (1.28)
Brain	2.11 (0.69)	2.07 (0.71)	1.36 (0.37)	1.16 (0.39)
		[^{125}I]**13**		
Blood	4.07 (0.30)	1.60 (0.30)	1.26 (0.26)	0.80 (0.20)

Liver	17.69 (2.64)	16.77 (2.20)	13.42 (1.70)	8.17 (1.28)
Kidney	11.93 (1.83)	9.35 (0.46)	6.77 (0.83)	2.76 (0.45)
Intestine	1.97 (0.22)	5.76 (0.66)	11.32 (1.65)	18.98 (3.21)
Spleen	7.56 (1.24)	7.09 (1.60)	4.75 (0.82)	2.39 (0.52)
Pancreas	5.55 (1.00)	5.59 (0.56)	3.57 (0.40)	2.22 (0.29)
Heart	12.91 (2.16)	5.84 (0.36)	2.97 (0.62)	1.36 (0.17)
Stomach[b]	0.97 (0.31)	1.97 (1.05)	2.11 (0.26)	1.62 (0.44)
Brain	2.13 (0.54)	2.62 (0.21)	1.93 (0.18)	1.82 (0.35)

[a] Expressed as % injection dose per gram. Each value represents the mean (SD) for 2-5 animals.

[b] Expressed as % injected dose per organ.

II-i 1,3,4-DPOD 誘導体の合成

Scheme 4 に1,3,4-DPOD誘導体の合成経路を示す。オキサジアゾール骨格の合成は以前に報告された方法で行った。4-Iodobenzohydrazide と 4-(dimethylamino)benzaldehyde を出発原料として、1段階の反応により、**22**を、4-iodobenzhydrazide と 4-methoxybenzealdehydeから**23**を得た。**23**の三臭化ホウ素による脱メチル化反応により**25**を49%の収率で得、**25**とnが1~3のエチレンオキシ鎖とをそれぞれ反応させることによって**26**、**27**、**28**を得た。**20**と**23**をそれぞれビストリメチルスズと反応させることによってスズ体である**21**、**24**を8.2%、6.5%の収率で得た。

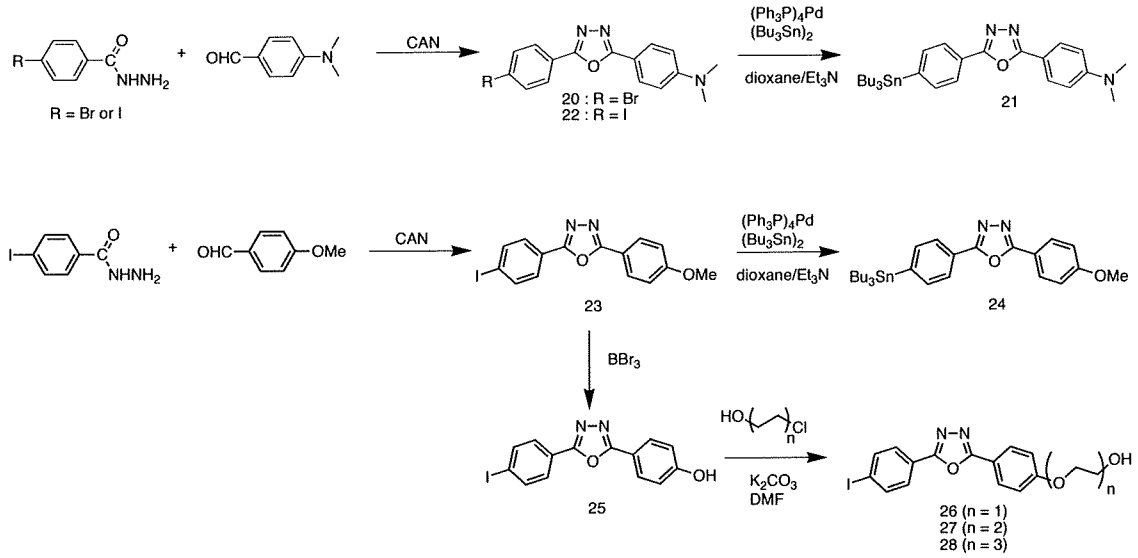

Scheme 4.

Ⅱ - ii　1,3,4-DPOD 誘導体の ^{125}I 標識

Scheme 5 に ^{125}I 標識経路を示す。目的とする[^{125}I]**22**、[^{125}I]**23** を放射化学的収率 45%以上、放射化学的純度 99%以上でそれぞれ得た。

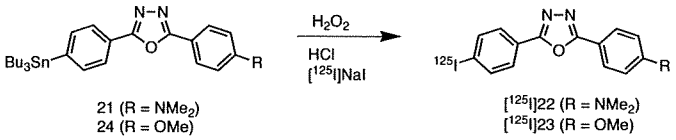

Scheme 5.

Ⅱ - iii　ジフェニルオキサジアゾール誘導体の Aβ(1-42)凝集体に対する結合親和性の検討

1,3,4-DPOD 誘導体の Ki 値は、20ー349 nM であり、Aβ凝集体に対し結合親和性を有することが示された。また、その結合性は導入した側鎖によって異なり、特に水酸基、エチレンオキシ鎖をそれぞれ導入した化合物 **25** ~ **28** は高い Ki 値を示した。このことより 1,3,4-DPOD の Aβ凝集体への結合性には、導入する側鎖が影響することが示唆された。また、1,3,4-DPOD 中でも最も高い結合親和性を示した化合物 **22** は以前に報告された 1,2,4-DPOD 誘導体にジメチルアミノ基を導入した 4-(3-(4-iodophenyl)-1,2,4-oxadiazole-5-yl)-*N,N*-dimethylamine (1,2,4-DPOD-DM, Ki = 15 nM)とほぼ同等の結合親和性を示した。

Table 3. Inhibition constants (K_i) for binding of 1,3,4-DPOD derivatives determined using [^{125}I]IMPY as the ligand in Aβ42 aggregates.

Compound	K_i (nM)[a]
22	20.1 ± 2.5
23	46.1 ± 12.6
25	229.6 ± 47.3
26	282.2 ± 61.4
27	348.6 ± 51.7
28	257.7 ± 34.8

[a]Values are the mean ± standard error for the mean for 4-6 independent experiments.

Ⅱ-iv Tg2576 トランスジェニックマウス脳切片を用いた蛍光染色

化合物 **22** を用いて、Tg2576 トランスジェニックマウス脳切片の蛍光染色を行い、1,3,4-DPOD のアミロイド斑への結合性を確認した。また、蛍光染色を用いた切片の隣接切片を用いて、老人斑アミロイド蛍光染色試薬として知られているチオフラビンSによる蛍光染色を行い、アミロイド斑の存在を確認した。比較として、wild-type マウス脳切片を用いた蛍光染色も行った。その結果、Tg2576 マウス脳切片上には wild-type マウス脳切片上には認められない複数の蛍光像が観察され、その蛍光像は、チオフラビン S の蛍光像と一致した。この結果より、1,3,4-DPOD 誘導体である化合物 **22** がマウス脳内に蓄積したアミロイド斑に対して選択的結合性を有することが明らかになった。

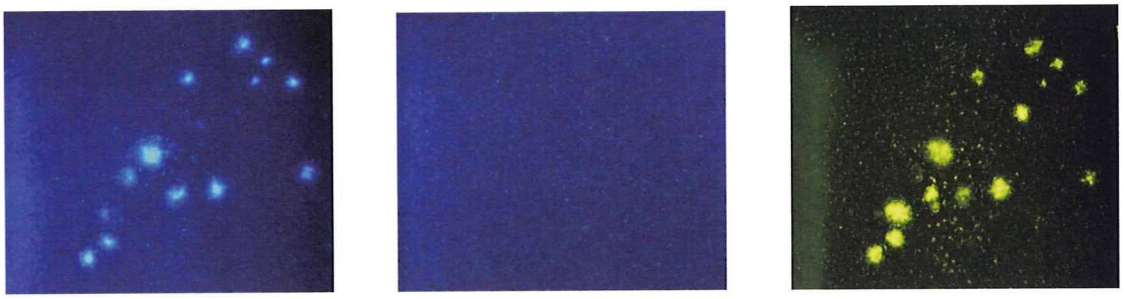

Figure 5. Neuropathological staining of compound **22** on 10-μm AD model mouse sections (left) and wild-type mouse sections (middle). Labeled plaques were confirmed by staining of the adjacent sections with thioflavin S (right).

Ⅱ-v 水／オクタノール間の分配係数測定による LogP 値の算出

1,3,4-DPOD 誘導体である[^{125}I]**22**、[^{125}I]**23** の LogP 値は、それぞれ 2.43、2.58 となり、1,2,4-DPOD 誘導体である[^{125}I]1,2,4-DPOD-DM 、[^{125}I]3-(4-iodophenyl)-5-(4-methoxyphenyl)-1,2,4-oxadiazole (1,2,4-DPOD-OMe) の LogP 値 3.22、3.37 より低い値を示した (Table 4)。また、[^{125}I]**22**、[^{125}I]**23** の LogP 値は血液脳関門の透過に必要であると報告されている、logP 値 1~3 の範囲内であることが示された。

Table 4. Partition coefficients for 1,2,4-DPOD and 1,3,4-DPOD derivatives.

Compound	log P^a
22	2.43 ± 0.07
23	2.58 ± 0.06
1,2,4-DPOD-DM	3.22 ± 0.01
1,2,4-DPOD-OMe	3.37 ± 0.04

[a]Octanol/buffer (0.1 M phosphate-buffered saline, pH 7.4) partition coefficients. Each value represents the mean (SD) for 2-3 experiments.

Ⅱ－vi　正常マウスを用いた体内放射能分布実験

5 週齢正常マウスを用いて 1,3,4-DPOD 誘導体の体内放射能分布実験を行った。[^{125}I]**22**、[^{125}I]**23** を正常マウスに投与後の脳における放射能挙動を、以前に報告された 1,2,4-DPOD 誘導体である[^{125}I]1,2,4-DPOD-DM、[^{125}I]1,2,4-DPOD-OMe の結果と併せて示す (Figure 5)。また、体内放射能分布の結果は Table 5 に示す。

1,2,4-DPOD 誘導体である[^{125}I]1,2,4-DPOD-DM、[^{125}I]1,2,4-DPOD-OMe は、脳への取り込みが遅く、その後の放射能は滞留傾向を示したのに対して、1,3,4-DPOD 誘導体である[^{125}I]**22**、[^{125}I]**23** は投与早期にそれぞれ 3.7、5.9%の放射能が脳へ移行しその後、経時的な放射能消失を示した。この放射能挙動の相違の一因として、1,3,4-DPOD が 1,2,4-DPOD より低い脂溶性を有することが考えられた。

以上の結果より、DPOD 誘導体の脳への移行性とクリアランスにはオキサジアゾール環へのフェニル基の導入位置が重要であると考えられた。

Table 5. Biodistribution of radioactivity after injection of [^{125}I]1,3,4-DPOD derivatives in normal mice[a].

	Time after injection (min)			
Tissue	2	10	30	60
		[^{125}I]**3**		

Blood	3.28 (0.46)	3.51 (0.29)	2.53 (0.28)	2.21 (0.41)
Liver	15.87 (3.49)	19.12 (2.43)	12.64 (2.44)	10.01 (1.64)
Kidney	9.14 (1.60)	7.80 (0.64)	5.71 (1.35)	3.81 (0.64)
Intestine	2.28 (0.55)	11.34 (1.61)	12.58 (2.35)	16.22 (2.51)
Spleen	3.56 (0.96)	4.10 (0.40)	2.63 (0.54)	2.05 (0.41)
Pancreas	5.32 (0.98)	4.39 (2.17)	2.50 (0.56)	2.14 (0.90)
Heart	3.99 (3.10)	3.55 (1.86)	2.03 (0.30)	1.54 (0.31)
Stomach[b]	1.40 (0.10)	4.73 (1.86)	4.79 (1.12)	5.50 (0.51)
Brain	2.98 (0.53)	5.93 (0.76)	3.16 (0.69)	1.78 (0.41)
		[^{125}I]**4**		
Blood	1.84 (0.30)	1.60 (0.30)	1.26 (0.26)	0.80 (0.20)
Liver	9.60 (1.73)	12.60 (1.14)	8.07 (1.66)	4.65 (1.34)
Kidney	7.14 (1.46)	4.85 (0.48)	4.36 (1.12)	2.48 (0.37)
Intestine	2.07 (0.36)	4.49 (0.60)	10.06 (1.81)	19.85 (4.71)
Spleen	2.44 (0.28)	1.51 (0.26)	0.80 (0.10)	0.60 (0.26)
Pancreas	4.74 (0.63)	1.98 (0.37)	0.96 (0.03)	0.57 (0.14)
Heart	4.80 (1.33)	1.73 (0.27)	0.92 (0.25)	0.43 (0.11)
Stomach[b]	0.71 (0.13)	1.41 (0.91)	3.12 (0.90)	2.90 (1.57)
Brain	3.75 (0.78)	2.74 (0.37)	1.04 (0.14)	0.36 (0.13)

[a]Expressed as % injection dose per gram. Each value represents the mean (SD) for 4-6 animals.

[b]Expressed as % injected dose per organ.

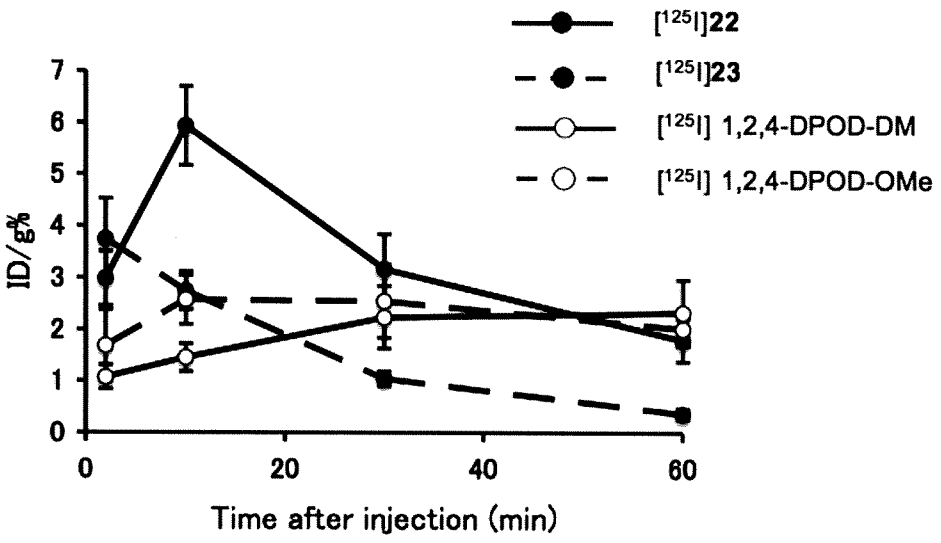

Figure 6. Comparison of brain uptake of [^{125}I]**22**, [^{125}I]**23**, [^{125}I]1,2,4-DPOD-DM and [^{125}I]1,2,4-DPOD-OMe in normal mice. The kinetics of the uptake of [^{125}I]1,3,4-DPOD-DM and [^{125}I]1,3,4-DPOD-OMe may provide a better pattern for the localization of Aβ plaques in the brain.

本研究において、AD の早期診断を目的とした新規 SPECT 用アミロイドイメージングプローブとして、フェニルインドールおよびジフェニルオキサジアゾールを基本骨格とした種々の ^{125}I 標識体の設計·合成およびその基礎的評価を行い、以下に述べる知見を得た。

(1) 種々の置換基を導入した5種の2-PI誘導体、1種の1-PI誘導体および6種の1,3,4-DPOD誘導体を合成することに成功した。

(2) Aβ(1-42)凝集体を用いたインビトロ結合実験において、インドール骨格の2位にフェニル基を導入した2-PIは側鎖に導入した置換基に関わらず、Aβ凝集体に対し高い結合親和性を示したのに対してインドール骨格の1位にフェニル基を導入した1-PIはAβ凝集体に対して、顕著な結合親和性を示さなかった。1,3,4-DPOD誘導体はいずれの化合物もAβ凝集体に対して結合親和性を示したが、導入した側鎖によって結合性には変化が見られた (Ki = 20 ~ 349 nM)。また、化合物**22**はこれまでに我々が報告してきた1,2,4-DPOD-DMとほぼ同等の結合性を示した。

(3) Tg2576脳切片を用いた蛍光染色において、2-PI誘導体である化合物**8**、1,3,4-DPOD誘導体である化合物**22**は、インビトロ結合実験の結果を反映して、アミロイド斑への結合性を示した。

(4) 正常マウスを用いた体内放射能分布実験において2-PIは脳への移行性を示したものの、クリアランスが遅く、脳内での滞留性が示唆された。この結果は、これまでに報告されてきたチオフラビンT 類似構造を基本骨格とした放射性ヨウ素標識体と類似したものだった。

(5) 正常マウスを用いた体内放射能分布実験において1,3,4-DPODは1,2,4-DPODと比較して投与早期の高い脳取り込みと速やかな脳からの放射能消失を示した。この放射能挙動の相違の一因として、1,3,4-DPODが1,2,4-DPODより低い脂溶性を有することが考えられた。

以上の結果より、2-PI および 1,3,4-DPOD は今後のアミロイドイメージングプローブの開発において有用な基本骨格となることが示された。

D. 考察

NSAIDs を基盤分子とする数種類の新規 SPECT 用プローブを設計・合成した。アミロイド凝集体を用いたインビトロ結合実験において、ジフェニルオキサジアゾール誘導体化合物３６と化合物３７は、アミロイド凝集体に対する高い結合親和性を示した。アルツハイマー病モデルマウス脳切片を用いた蛍光染色実験より、化合物および化合物は、脳への高い移行性を示した。今後、ジフェニルオキサジアゾール骨格へ更なる分子修飾を行い、高性能なアミロイドイメージングプローブの開発を推進していくとともに、アミロイドイメージングプローブとなりうる NSAIDs を基盤分子とした新規リード化合物を探索していく予定である。

E. 結論

NSAIDs を基盤分子とする放射性ヨウ素標識化合物の中から、ジフェニルオキサジアゾール骨格が新規 SPECT 用アミロイドイメージングプローブとして機能することが示唆された。また、本結果は NSAIDs を基盤分子としたアミロイドイメージングプローブ開発の妥当性を示すものであり、今後更なるリード化合物の探索研究の必要性が示唆された。

F. 健康危険情報

なし

G. 研究発表

Ono M, Haratake M, Saji H, Nakayama M. Development of novel β-amyloid probes based on 3,5-diphenyl-1,2,4-oxadiazole. Bioorganic&Medicinal Chemistry, 16, 6867-72, 2008.

小野正博、佐治英郎、PET/SPECT によるβアミロイドの分子イメージングーアルツハイマー病の早期診断を目指して, 化学, 63, 64-65, 2008.

小野正博、PET/SPECT を用いたアルツハイマー病の画像診断、薬剤学、68, 427-424, 2008.

Maya Y, Ono M, Watanabe H, Haratake M, Saji H, Nakayama M. Novel radioiodinated aurones as probes for SPECT imaging of b-amyloid plaques in the brain. *Bioconjugate Chemistry*, **20**, 95-101 (2009).

Ono M, Watanabe R, Kawashima H, Kawai T, Watanabe H, Haratake M, Saji H, Nakayama M. ^{18}F-labeled flavones for *in vivo* imaging of b-amyloid plaques in Alzheimer's brains. *Bioorganic and*

Medicinal Chemistry, **17**, 2069-2076 (2009).

Watanabe H, Ono M, Ikeoka R, Haratake M, Saji H, Nakayama M. Synthesis and biological evaluation of radioiodinated 2,5-diphenyl-1,3,4-oxadiazoles for detecting b-amyloid plaques in the brain. *Bioorganic and Medicinal Chemistry*, **17**, 6402-6406 (2009).

Ono M, Hayashi S, Kimura H, Kawashima H, Nakayama M, Saji H. Push-pull benzothiazole derivatives as probes for detecting b-amyloid plaques in Alzheimer's brains. *Bioorganic and Medicinal Chemistry*, **17**, 7002-7009 (2009).

Ono M, Watanabe R, Kawashima H, Cheng Y, Kimura H, Watanabe H, Haratake M, Saji H, Nakayama M. Fluoro-pegylated chalcones as positron emission tomography probes for in vivo imaging of β-amyloid plaques in Alzheimer's disease. *Journal of Medicinal Chemistry*, **52**, 6394-6401 (2009).

Ono M. Molecular imaging by PET/SPECT. *Yakugaku Zasshi*, **129**, 279-287 (2009).

Ono M. Development of positron-emission tomography/single-photon emission computed tomography imaging probes for in vivo detection of b-amyloid plaques in Alzheimer's brains. *Chemical & Pharmaceutical Bulletin*, **57**, 1029-1039 (2009).

H. 知的財産権の出願・登録状況

特願 2008-043750、ジフェニルオキサジアゾール誘導体含有診断用組成物、小野正博、中山守雄、長崎大学、平成２０年２月２６日

特願 2009-37773、佐治 英郎、小野 正博、河嶋 秀和、木村 寛之、ベンゾチアゾール誘導体含有診断用組成物、京都大学、平成２１年２月２０日

特願 2009-50186、テクネチウム標識化合物含有診断用組成物、中山 守雄、原武 衛、小野 正博、長崎大学、平成２１年３月４日

特願 2009-107457、佐治 英郎、小野正博、コンフォメーション病診断用組成物、京都大学、平成２１年４月２７日

特願 2009-222156、佐治 英郎、小野

正博、木村 寛之、河嶋 秀和、コンフォメーション病診断のための組成物、　京都大学、平成２１年９月２８日

研究成果の刊行に関する一覧表

書籍

氏名	論文タイトル名	書籍全体の編集者名	書　籍　名	出版社名	出版地	出版年	ページ
なし							

雑誌

発表者氏名	論文タイトル名	発表誌名	巻号	ページ	出版年
Ono M, Haratake M, Saji H, Nakayama M	Development of novel β-amyloid probes based on 3,5-diphenyl-1,2,4-oxadiazole	Bioorganic& Medicinal Chemistry	16	6867-6872	2008
小野正博, 佐治英郎	PET/SPECT によるβアミロイドの分子イメージングーアルツハイマー病の早期診断を目指して	化学	63	64-65	2008
小野正博	PET/SPECT を用いたアルツハイマー病の画像診断	薬剤学	68	427-434	2008
Maya Y, Ono M, Watanabe H, Haratake M, Saji H, Nakayama M	Novel radioiodinated aurones as probes for SPECT imaging of β-amyloid plaques in the brain.	Bioconjugate Chemistry	20	95-101	2009
Ono M, Watanabe R, Kawashima H, Kawai T, Watanabe H, Haratake M, Saji H, Nakayama M.	^{18}F-labeled flavones for *in vivo* imaging of β-amyloid plaques in Alzheimer's brains	Bioorganic& Medicinal Chemistry	17	2069-2076	2009
Watanabe H, Ono M, Ikeoka R, Haratake M, Saji H, Nakayama M	Synthesis and biological evaluation of radioiodinated 2,5-diphenyl-1,3,4-oxadiazole for detecting β-amyloid plaques in the brain.	Bioorganic& Medicinal Chemistry	17	6402-6406	2009

Ono M, Hayashi S, Kimura H, Kawashima H, Nakayama M, Saji H	Push-pull benzothiazole derivatives as probes for detecting β-amyloid plaques in Alzheimer's brains.	Bioorganic& Medicinal Chemistry	17	7002-7007	2009
Ono M, Watanabe R, Kawashima H, Cheng Y, Kimura H, Watanabe H, Haratake M, Saji H, Nakayama M.	Fluoro-pegylated chalcones as positron emission tomography probes for in vivo imaging of β-amyloid plaques in Alzheimer's disease.	Journal of Medicinal Chemistry	52	6394-6401	2009
小野正博	PET/SPECT による分子イメージング研究	薬学雑誌	129	279-287	2009
Ono M	Development of positron-emission tomography/ single-photon emission computed tomography imaging probes for in vivo detection of β-amyloid plaques in Alzheimer's brains.	Chemical & Pharmaceutical Bulletin	57	1029-1039	2009

Bioorganic & Medicinal Chemistry 16 (2008) 6867–6872

Contents lists available at ScienceDirect

Bioorganic & Medicinal Chemistry

journal homepage: www.elsevier.com/locate/bmc

Development of novel β-amyloid probes based on 3,5-diphenyl-1,2,4-oxadiazole

Masahiro Ono [a,b,*], Mamoru Haratake [a], Hideo Saji [b], Morio Nakayama [a]

[a] Graduate School of Biomedical Sciences, Nagasaki University, 1-14 Bunkyo-machi, Nagasaki 852-8521, Japan
[b] Graduate School of Pharmaceutical Sciences, Kyoto University, 46-29 Yoshida Simoadachi-cho, Sakyo-ku, Kyoto 606-8501, Japan

ARTICLE INFO

Article history:
Received 1 May 2008
Revised 23 May 2008
Accepted 24 May 2008
Available online 29 May 2008

Keywords:
Alzheimer's disease
β-Amyloid
PET
SPECT

ABSTRACT

In the search for novel probes for the imaging in vivo of β-amyloid plaques in Alzheimer's disease (AD) brain, we have synthesized and evaluated a series of 3,5-diphenyl-1,2,4-oxadiazole (DPOD) derivatives. The affinity for β-amyloid plaques was assessed by an in vitro-binding assay using pre-formed synthetic Aβ42 aggregates. The new series of DPOD derivatives showed excellent affinity for Aβ aggregates with K_i values ranging from 4 to 47 nM. In biodistribution experiments using normal mice, [^{125}I]**12**, [^{125}I]**13**, [^{125}I]**14**, and [^{125}I]**15** examined displayed sufficient uptake for imaging, ranging from 2.2 to 3.3% ID/g. But the washout of the four ligands from the brain was relatively slow. Although additional modifications are necessary to improve the uptake and rapid clearance of non-specifically bound radiotracers, the DPOD pharmacophore with high-binding affinity for Aβ aggregates may be useful as a backbone structure to develop novel β-amyloid imaging agents.

1. Introduction

Alzheimer's disease (AD) is the most common neurodegenerative disorder of the elderly and is characterized clinically by dementia, cognitive impairment, and memory loss. The neuropathological hallmarks of AD include abundant deposits of β-amyloid plaques and neurofibrillary tangles. The deposition of β-amyloid plaques has been regarded as an initial event in the pathogenesis of AD.[1,2] Therefore, the quantitative evaluation of β-amyloid plaques in the brain with non-invasive techniques such as positron emission tomography (PET) and single photon emission computed tomography (SPECT) could lead to the presymptomatic detection of AD and new anti-amyloid therapies.[3–5]

Developing β-amyloid imaging probes is currently an emerging field of research. The basic requirements for suitable probes include (i) good penetration of the blood–brain barrier, (ii) selectively binding or labeling β-amyloid plaques, and (iii) displaying clear and contrasting signals between plaques and non-plaques. Based on these requirements, several promising agents with the backbone structure of DDNP, thioflavin-T, and Congo Red have been synthesized and evaluated for use in vivo as probes to image β-amyloid plaques in AD brain. Clinical trials in AD patients have been conducted with several agents including [^{18}F]FDDNP,[6,7] [^{11}C]6-OH-BTA-1,[8,9] [^{11}C]SB-13,[10,11] [^{18}F]BAY94-9172,[12] and [^{123}I]IMPY[13,14] (Fig. 1) indicating the imaging of β-amyloid plaques in the living human brain to be useful for the diagnosis of AD.

Recently, a number of groups have reported new β-amyloid-binding probes without the basic structures of DDNP, thioflavin-T and Congo Red. Most of these probes have two aromatic rings. Among them, 1,4-diphenyltriazole and 2,5-diphenylthiophene derivatives have triazole and thiophene between two benzene rings, respectively, and it has been shown that they have tolerance for binding to Aβ aggregates.[15,16] In an attempt to further develop novel ligands for the imaging of amyloid plaques in AD, we designed a series of 3,5-diphenyl-1,2,4-oxadiazole (DPOO) derivatives, in which triazole or thiophene of the 1,4-diphenyltriazole and 2,5-diphenylthiophene backbone was replaced with 1,2,4-oxadiazole. To our knowledge, this is the first time the use of DPOD derivatives in vivo as probes to image β-amyloid plaques in the AD brain has been proposed. Described herein is the synthesis of a novel series of DPOD derivatives and the characterization as β-amyloid imaging agents.

2. Results and discussion

The synthesis of the DPOD derivatives is outlined in Schemes 1 and 2. A wide variety of reaction conditions have been published for the synthesis of 3,5-diphenyl-1,2,4-oxadiazoles.[17] Among them, we used the reaction of an amidoxime with a carboxylic acid to form 1,2,4-oxadiazoles. In this process, the 3,5-diphenyl-1,2,4,-oxadiazoles (**1** and **5**) were prepared by the condensation of 4-bromobenzamidoxime with 4-nitrobenzoic acid and 4-methoxybenzoic acid in the presence of DCC and HOBT. The amino derivative **2** was readily prepared from **1** by reduction with $SnCl_2$ (80.8% yield). Conversion of **2** to the monomethylamino derivative **3** was achieved by a method reported previously[18] (50.3% yield).

* Corresponding author. Tel.: +81 75 753 4608; fax: +81 75 753 4568.
E-mail address: ono@pharm.kyoto-u.ac.jp (M. Ono).

0968-0896/$ - see front matter © 2008 Elsevier Ltd. All rights reserved.
doi:10.1016/j.bmc.2008.05.054

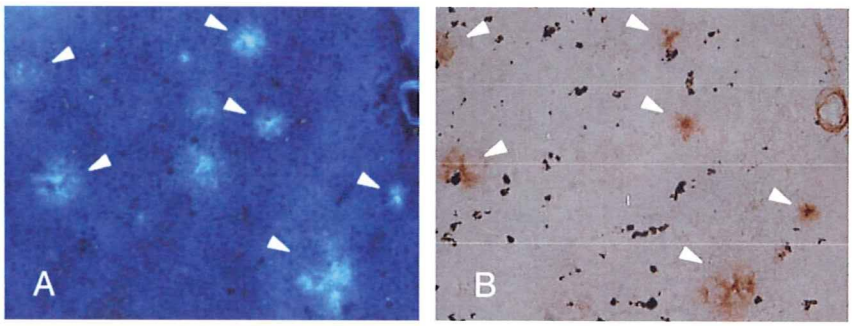

Figure 1. Neuropathological staining of compound **14** on 10-μm AD model mouse sections. (A) Many β-amyloid plaques were clearly stained with **14**. (B) The serial sections were immunostained using an antibody against β-amyloid.

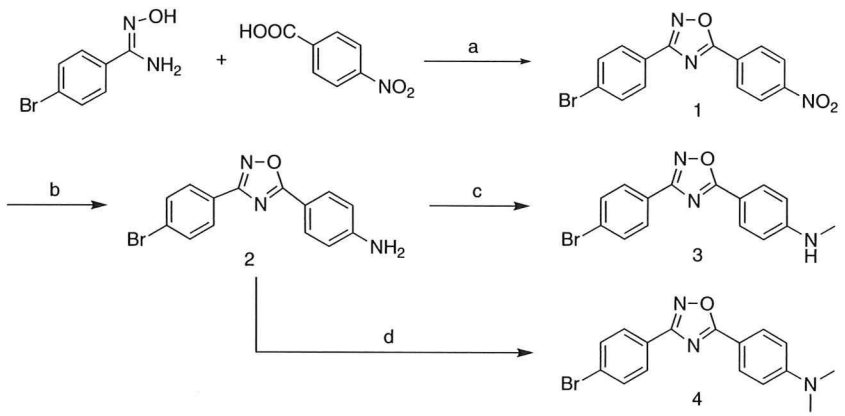

Scheme 1. (a) DCC, HOBT, DMF; (b) $SnCl_2$, EtOH; (c) NaOMe, $(CH_2O)_n$, $NaBH_4$, MeOH; (d) $(CH_2O)_n$, $NaCNBH_3$, AcOH.

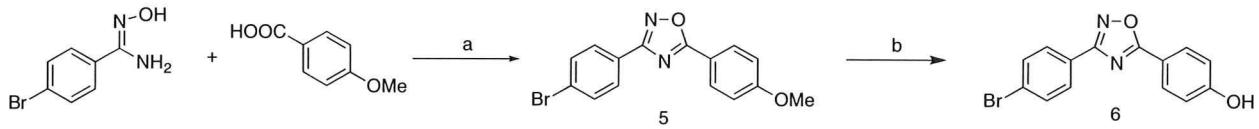

Scheme 2. (a) DCC, HOBT, DMF; (b) BBr_3, CH_2Cl_2.

Compound **2** was also converted to the dimethylamino derivative **4** by an efficient method[19] with paraformaldehyde and acetic acid (68.4% yield). Compound **5** was converted to **6** by demethylation with BBr_3 in CH_2Cl_2 (50.6% yield). The tributyltin derivatives (**7**, **8**, **9**, **10**, and **11**) were prepared from the corresponding bromo compounds (**2**, **3**, **4**, **5**, and **6**) using a bromo to tributyltin exchange reaction catalyzed by Pd(0) for yields of 16.8%, 15.8%, 20.3%, 22.8%, and 60.1%, respectively. These tributyltin derivatives were readily reacted with iodine in chloroform at room temperature to give the iodo derivatives (**12**, **13**, **14**, **15**, and **16**) for yields of 66.1%, 86.0%, 72.4%, 69.2%, and 81.8%. Furthermore, these tributyltin derivatives can be also used as the starting materials for radioiodination in the preparation of [^{125}I]**12**, [^{125}I]**13**, [^{125}I]**14**, and [^{125}I]**15**. Novel radioiodinated DPOD derivatives were achieved by an iododestannylation reaction using hydrogen peroxide as the oxidant which produced the desired radioiodinated ligands (Scheme 3). It was anticipated that the no-carrier-added preparation would result in a final product bearing a theoretical specific activity similar to that of ^{125}I (2200 Ci/mmol). The radiochemical identities of the radioiodinated ligands were verified by co-injection with non-radioactive compounds from their HPLC profiles. The final radioiodinated compounds, [^{125}I]**12**, [^{125}I]**13**, [^{125}I]**14**, and [^{125}I]**15**, showed a single peak of radioactivity at a retention time of 8.4, 15.7, 25.5, 22.3, and 7.1 min, respectively. Four radioiodinated products were obtained in 50–70% radiochemical yields with a radiochemical purity of >95% after HPLC.

The affinity of DPOD derivatives (compounds **12**, **13**, **14**, **15**, and **16**) was evaluated based on inhibition of the binding of [^{125}I]IMPY to Aβ(1–42) aggregates. As shown in Table 1, all the derivatives competed well with [^{125}I]IMPY to bind the aggregates. The K_i values estimated for **12**, **13**, **14**, **15**, and **16** were 14, 14, 15, 4, and 47 nM, respectively. The introduction into the DPOD backbone of an aminophenyl moiety, such as aminophenyl, methylaminophenyl or dimethylaminophenyl, resulted in good affinity. Further modification of the aminophenyl moiety with another electron-donating group, such as methoxyphenyl or hydroxyphenyl, resulted in a difference in binding to Aβ aggregates, with the methoxy derivative **15** having 10-fold higher affinity than the hydroxy derivative **16**.

To confirm the affinity of DPOD derivatives for β-amyloid plaques in the AD brain, fluorescent staining of sections of mouse brain from an animal model of AD was carried out with compound **14** (Fig. 1). Many β-amyloid plaques were clearly stained with compound **14**, as reflected by the affinity for Aβ aggregates in in vitro competition assays. The labeling pattern was consistent with that observed by immunohistochemical labeling with an antibody specific for Aβ, indicating that DPOD derivatives show specific binding to β-amyloid plaques. Thus, the results suggest that DPOD

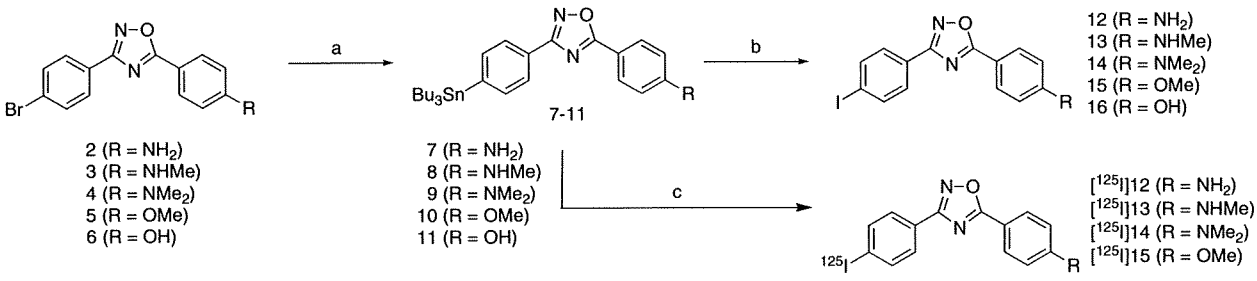

Scheme 3. $(Bu_3Sn)_2$, $Pd(PhP_3P)$, Et_3N, dioxane; (b) I_2, $CHCl_3$; (c) [^{125}I]NaI, H_2O_2, HCl.

Table 1
Inhibition constants for the binding of DPOD derivatives determined using [^{125}I]IMPY as the ligand in Aβ(1–42) aggregates

Compound	K_i[a] (nM)
12	14.2 ± 1.4
13	14.3 ± 3.6
14	15.4 ± 1.4
15	4.3 ± 2.1
16	47.1 ± 4.1

[a] Values are means ± standard error of the mean for 3–6 independent experiments.

Table 2
Biodistribution of radioactivity after intravenous administration of [^{125}I]**12**, [^{125}I]**13**, [^{125}I]**14**, and [^{125}I]**15** in mice[a]

Tissue	Time after injection (min)			
	2	10	30	60
[^{125}I]**12**				
Blood	4.55 (0.64)	2.32 (0.63)	3.09 (0.22)	2.99 (0.31)
Liver	21.36 (3.13)	17.37 (1.72)	14.89 (1.47)	12.33 (2.19)
Kidney	8.24 (1.26)	6.94 (0.70)	5.86 (0.56)	5.15 (0.74)
Intestine	1.50 (0.36)	3.08 (0.47)	5.84 (0.75)	8.33 (1.39)
Spleen	6.13 (1.67)	8.87 (2.35)	6.89 (0.81)	5.02 (0.55)
Pancreas	3.69 (2.30)	3.88 (0.54)	3.36 (0.36)	2.83 (0.32)
Heart	9.29 (1.66)	4.02 (0.48)	3.48 (0.24)	3.51 (0.61)
Stomach[b]	0.92 (0.31)	1.70 (0.18)	4.05 (0.96)	5.15 (1.32)
Brain	1.61 (0.23)	2.48 (0.16)	3.32 (0.31)	3.29 (0.58)
[^{125}I]**13**				
Blood	3.54 (0.26)	1.84 (0.24)	1.52 (0.13)	1.54 (0.09)
Liver	14.62 (1.30)	12.37 (2.09)	8.53 (0.98)	7.30 (0.78)
Kidney	9.53 (0.83)	5.30 (0.94)	3.39 (0.66)	3.02 (0.58)
Intestine	1.36 (0.21)	2.83 (0.93)	5.67 (1.44)	8.46 (1.36)
Spleen	4.58 (0.62)	4.70 (0.48)	2.84 (0.35)	2.14 (0.22)
Pancreas	3.34 (0.38)	3.91 (0.60)	3.06 (0.58)	1.88 (0.25)
Heart	9.51 (0.77)	3.05 (0.50)	1.68 (0.21)	1.27 (0.20)
Stomach[b]	1.08 (0.11)	2.32 (0.62)	4.89 (0.99)	7.38 (0.97)
Brain	1.44 (0.12)	1.98 (0.36)	2.56 (0.44)	2.70 (0.33)
[^{125}I]**14**				
Blood	5.42 (0.85)	2.41 (0.22)	1.79 (0.24)	1.56 (0.27)
Liver	13.94 (3.26)	8.27 (1.49)	5.89 (1.75)	5.15 (1.92)
Kidney	7.83 (3.53)	7.67 (1.62)	4.81 (1.01)	3.31 (0.77)
Intestine	1.59 (0.28)	2.40 (0.36)	4.12 (0.99)	5.37 (1.01)
Spleen	6.26 (1.53)	4.56 (1.11)	3.11 (0.62)	2.41 (0.29)
Pancreas	3.17 (0.73)	3.80 (0.50)	2.86 (1.64)	2.47 (0.62)
Heart	11.04 (2.43)	4.81 (1.07)	2.20 (0.54)	1.24 (0.68)
Stomach[b]	1.28 (0.21)	3.28 (0.36)	4.80 (0.56)	5.75 (2.47)
Brain	1.07 (0.23)	1.45 (0.27)	2.23 (0.61)	2.32 (0.64)
[^{125}I]**15**				
Blood	1.96 (0.66)	1.63 (0.14)	1.23 (0.39)	1.12 (0.26)
Liver	11.94 (1.92)	9.35 (1.17)	6.13 (0.76)	4.44 (0.60)
Kidney	8.77 (1.17)	6.22 (0.87)	3.85 (1.01)	2.95 (0.66)
Intestine	1.70 (0.27)	3.53 (0.32)	6.62 (0.90)	8.21 (1.84)
Spleen	4.41 (0.72)	3.62 (0.28)	2.13 (0.53)	1.34 (0.40)
Pancreas	4.55 (0.77)	4.94 (0.26)	2.84 (0.48)	1.45 (0.28)
Heart	11.30 (1.92)	4.44 (0.67)	1.84 (0.32)	1.35 (0.29)
Stomach[b]	0.62 (0.21)	1.64 (0.10)	2.46 (0.80)	3.16 (1.39)
Brain	2.06 (0.45)	2.76 (0.23)	2.82 (0.34)	2.01 (0.33)

[a] Expressed as % injected dose per gram. Each value represents the mean (s.d.) for 3–5 animals at each interval.
[b] Expressed as % injected dose per organ.

derivatives may be applicable to the in vivo imaging of β-amyloid plaques in the brain.

To evaluate the uptake of DPOD derivatives in the brain, biodistribution experiments in normal mice were performed with four radioiodinated DPOD derivatives ([^{125}I]**12**, [^{125}I]**13**, [^{125}I]**14**, and [^{125}I]**15**), which showed strong affinity for Aβ aggregates in the in vitro-binding assays (Table 2). All four ligands penetrated the brain well with a delayed peak time at 30 and 60 min for uptakes (2.3–3.3%ID/g brain) in normal mice. But as a prerequisite for an imaging agent, they should be washed out from the normal brain, because there is no trapping mechanism for DPOD derivatives. Nevertheless, the long retention of these probes in the normal mouse brain suggested extensive non-specific binding which will contribute to a high level of background noise in vivo. Previously, we reported radioiodinated benzofuran derivatives as potential β-amyloid-binding agents.[20] The radioiodinated benzofurans penetrated the brain well with a peak uptake at 30–60 min postinjection, but a slow washout in normal mice prevents these probes from being used for imaging in vivo. More recently, we developed ^{11}C-labeled benzofuran derivatives, which are less lipophilic by replacing the iodine with a hydroxy group.[21] [^{11}C]benzofuran showed a higher and faster peak of brain uptake and a faster washout from the brain in the normal mice. The improved properties in vivo observed with [^{11}C]benzofuran make it a better candidate for the imaging of β-amyloid plaques. Indeed, the initial result obtained with [^{11}C]benzofuran in a transgenic2576 mouse showed a relatively high S/N ratio.[21] Similar to [^{125}I]benzofuran, the DPOD derivatives had unfavorable in vivo pharmacokinetics in normal mice, despite their good affinity for Aβ aggregates. Additional structural changes, that is, reducing the lipophilicity by introducing a hydrophilic group, are necessary to improve the in vivo properties of the DPOD derivatives.

3. Conclusion

In conclusion, we successfully designed and synthesized a new series of DPOD derivatives as probes for the in vivo imaging of β-amyloid plaques in the brain. The derivatives displayed excellent affinity for Aβ aggregates in in vitro-binding experiments. The degree to which the DPOD derivatives penetrated the brain was also very encouraging. However, non-specific binding in vivo reflected by a slow washout from the normal mouse brain makes them unsuitable for the imaging of β-amyloid plaques. The less than ideal in vivo biodistribution results in normal mice indicate that there is a critical need to fine-tune the kinetics of brain uptake and washout. Additional changes to the DPOD pharmacopore with

high-binding affinity for Aβ aggregates may lead to useful probes for detecting β-amyloid plaques in the AD brain.

4. Experimental

4.1. General information

All reagents were commercial products and used without further purification unless otherwise indicated. ^{1}H NMR spectra were obtained on a Varian Gemini 300 spectrometer with TMS as an internal standard. Coupling constants are reported in Hertz. Multiplicity is defined by s (singlet), d (doublet), t (triplet), br (broad), and m (multiplet). Mass spectra were obtained on a JEOL IMS-DX instrument.

4.1.1. 3-(4-Bromophenyl)-5-(4-nitrophenyl)-1,2,4-oxadiazole (1)

To a stirring solution of 4-bromobenzamidoxime (645 mg, 3 mmol) and 4-nitrobenzoic acid (495 mg, 3 mmol) in DMF (10 mL) was added a solution of DCC (3.6 mmol) and HOBT (6.0 mmol) in DMF (5 mL). The reaction mixture was stirred at room temperature for 18 h, and then at 100 °C for 2 h. The solvent was removed, and the residue was purified by silica gel chromatography (hexane/ethyl acetate = 9:1) to give 370 mg of **1** (35.6%). ^{1}H NMR (300 MHz, $CDCl_3$) δ 7.70 (d, J = 8.7 Hz, 2H), 8.06 (d, J = 8.7 Hz, 2H), and 8.43 (s, 4H). MS m/z 346 (M^+).

4.1.2. 4-(3-(4-Bromophenyl)-1,2,4-oxadiazol-5-yl)aniline (2)

A mixture of **1** (350 mg, 1 mmol), $SnCl_2$ (948 mg, 5 mmol) and EtOH (15 mL) was stirred under reflux for 2 h. After the mixture had cooled to room temperature, 1 M NaOH (100 mL) was added until the mixture became alkaline. After extraction with ethyl acetate (100 mL × 2), the combined organic layer was washed with brine, dried over Na_2SO_4, and evaporated to give 258 mg of **2** (80.8%). ^{1}H NMR (300 MHz, $CDCl_3$) δ 4.16 (s, 2H), 6.75 (d, J = 8.7 Hz, 2H), 7.63 (d, J = 8.4 Hz, 2H), 8.00 (d, J = 9.0 Hz, 2H), and 8.03 (d, J = 6.3 Hz, 2H). MS m/z 316 (M^+).

4.1.3. 4-(3-(4-Bromophenyl)-1,2,4-oxadiazol-5-yl)-*N*-methylaniline (3)

A solution of $NaOCH_3$ (28 wt% in MeOH, 0.4 mL) was added to a mixture of **2** (185 mg, 0.59 mmol) and paraformaldehyde (176 mg, 0.59 mmol) in methanol (10 mL) dropwise. The mixture was stirred under reflux for 30 min. After $NaBH_4$ (225 mg, 5.9 mmol) was added, the solution was heated under reflux for 1.5 h. 1 M NaOH (50 mL) was added to the cold mixture and extracted with $CHCl_3$ (50 mL). The organic phase was dried over Na_2SO_4 and filtered. The solvent was removed, and the residue was purified by silica gel chromatography (hexane/ethyl acetate = 4:1) to give 98 mg of **3** (50.3%). ^{1}H NMR (300 MHz, $CDCl_3$) δ 2.93 (s, 3H), 4.30 (s, 1H), 6.66 (d, J = 8.7 Hz, 2H), 7.63 (d, J = 8.7 Hz, 2H), 8.01 (d, J = 8.7 Hz, 2H), and 8.03 (d, J = 8.7 Hz, 2H). MS m/z 330 (M^+).

4.1.4. 4-(3-(4-Bromophenyl)-1,2,4-oxadiazol-5-yl)-*N*,*N*-dimethylaniline (4)

To a stirred mixture of **2** (35 mg, 0.10 mmol) and paraformaldehyde (36 mg, 1.2 mmol) in AcOH (5 mL) was added $NaCNBH_3$ (50 mg, 0.80 mmol) in one portion at room temperature. The resulting mixture was stirred at room temperature for 2 h. After 1 M NaOH (30 mL) was added and extraction with CH_3Cl (30 mL), the organic phase was dried over Na_2SO_4. The solvent was removed and the residue was purified by silica gel chromatography (hexane/ethyl acetate = 4:1) to give 24 mg of **4** (68.4%). ^{1}H NMR (300 MHz, $CDCl_3$) δ 3.09 (s, 6H), 6.75 (d, J = 9.0 Hz, 2H), 7.63 (d, J = 8.4 Hz, 2H), 8.35 (d, J = 8.7 Hz, 2H), and 8.43 (d, J = 8.7 Hz, 2H). MS m/z 344.

4.1.5. 3-(4-Bromophenyl)-5-(4-methoxyphenyl)-1,2,4-oxadiazole (5)

The same reaction as described above to prepare **1** was used, and 153 mg of **5** was obtained in a 23.1% yield from 4-bromobenzamidoxime and 4-anisic acid. ^{1}H NMR (300 MHz, $CDCl_3$) δ 3.91 (s, 3H), 7.05 (d, J = 8.7 Hz, 2H), 7.65 (d, J = 8.7 Hz, 2H), 8.04 (d, J = 8.4 Hz, 2H), 8.15 (d, J = 9.0 Hz, 2H). MS m/z 330 (M^+).

4.1.6. 4-(3-(4-Bromophenyl)-1,2,4-oxadiazol-5-yl)phenol (6)

BBr_3 (4.5 mL, 1 M solution in CH_2Cl_2) was added to a solution of **5** (300 mg, 0.91 mmol) in CH_2Cl_2 (10 mL) dropwise in an ice bath. The mixture was allowed to warm to room temperature and stirred for 42 h. Water (30 mL) was added while the reaction mixture was cooled in an ice bath. The mixture was extracted with chloroform (30 mL × 2) and the organic phase was dried over Na_2SO_4 and filtered. The solvent was removed and the residue was purified by silica gel chromatography (hexane/ethyl acetate = 4:1) to give 146 mg of **6** (50.6%). ^{1}H NMR (300 MHz, $CDCl_3$) δ 6.99 (d, J = 8.7 Hz, 2H), 7.65 (d, J = 8.7 Hz, 2H), 8.04 (d, J = 8.1 Hz, 2H), and 8.12 (d, J = 9.0 Hz, 2H). MS m/z 316 (M^+).

4.1.7. 4-(3-(4-(Tributylstannyl)phenyl)-1,2,4-oxadiazol-5-yl)aniline (7)

A mixture of **2** (100 mg, 0.32 mmol), bis(tributyltin) (0.2 mL) and $(Ph_3P)_4Pd$ (16 mg, 0.014 mmol) in a mixed solvent (10 mL, 3:2 dioxane/triethylamine mixture) was stirred for 10 h under reflux. The solvent was removed, and the residue was purified by silica gel chromatography (hexane/ethyl acetate = 3:1) to give 28 mg of **7** (16.8%). ^{1}H NMR (300 MHz, $CDCl_3$) δ 0.87–1.61 (m, 27H), 4.13 (s, 2H), 6.76 (d, J = 8.7 Hz, 2H), 7.59 (d, J = 8.1 Hz, 2H), 8.01 (d, J = 8.7 Hz, 1H), 8.07 (d, J = 8.1 Hz, 2H), and 8.28 (s, 1H).

4.1.8. *N*-Methyl-4-(3-(4-(tributylstannyl)phenyl)-1,2,4-oxadiazol-5-yl)aniline (8)

The same reaction as described above to prepare **7** was employed, and 23 mg of **8** was obtained in a 15.8% yield from **3**. ^{1}H NMR (300 MHz, $CDCl_3$) δ 0.87–1.63 (m, 27H), 2.92 (s, 3H), 4.27 (s, 1H), 6.66 (d, J = 8.7 Hz, 2H), 7.59 (d, J = 8.1 Hz, 2H), 8.03 (d, J = 8.4 Hz, 2H), and 8.08 (d, J = 7.8 Hz, 2H).

4.1.9. *N*,*N*-Dimethyl-4-(3-(4-(tributylstannyl)phenyl)-1,2,4-oxadiazol-5-yl)aniline (9)

The same reaction as described above to prepare **7** was employed, and 45 mg of **9** was obtained in a 20.3% yield from **4**. ^{1}H NMR (300 MHz, $CDCl_3$) δ 0.87–1.58 (m, 27H), 3.09 (s, 6H), 6.76 (d, J = 9.6 Hz, 2H), 7.59 (d, J = 8.1 Hz, 2H), 8.05 (d, J = 8.4 Hz, 2H), and 8.08 (d, J = 8.4 Hz, 2H).

4.1.10. 5-(4-Methoxyphenyl)-3-(4-(tributylstannyl)phenyl)-1,2,4-oxadiazole (10)

The same reaction as described above to prepare **7** was employed, and 42 mg of **10** was obtained in a 22.8% yield from **5**. ^{1}H NMR (300 MHz, $CDCl_3$) δ 0.87–1.59 (m, 27H), 3.91 (s, 3H), 7.04 (d, J = 8.7 Hz, 2H), 7.61 (d, J = 7.8 Hz, 2H), 8.07 (d, J = 9.0 Hz, 2H), and 8.17 (d, J = 9.0 Hz, 2H).

4.1.11. 4-(3-(4-(Tributylstannyl)phenyl)-1,2,4-oxadiazol-5-yl)phenol (11)

The same reaction as described above to prepare **7** was employed, and 28 mg of **11** was obtained in a 60.1% yield from **6**. ^{1}H NMR (300 MHz, $CDCl_3$) δ 0.87–1.58 (m, 27H), 6.99 (d, J = 9.0 Hz, 2H), 7.61 (d, J = 7.8 Hz, 2H), 8.07 (d, J = 8.7 Hz, 2H), and 8.12 (d, J = 8.7 Hz, 2H).

4.1.12. 4-(3-(4-Iodophenyl)-1,2,4-oxadiazol-5-yl)aniline (12)

To a solution of **7** (27 mg, 0.05 mmol) in $CHCl_3$ (5 mL) was added a solution of iodine in $CHCl_3$ (1 mL, 50 mg/mL) at room temperature. The mixture was stirred at room temperature for 10 min and a saturated $NaHSO_3$ solution (25 mL) was added. The mixture was stirred for 5 min and the organic phase was separated. The aqueous phase was extracted with CH_3Cl (25 mL × 2), and the combined organic phase was dried over Na_2SO_4 and filtered. The solvent was removed and the residue was washed with hexane to give 12 mg of **12** (66.1%). ^1H NMR (300 MHz, $CDCl_3$) δ 4.15 (s, 2H), 6.76 (d, J = 8.7 Hz, 2H), 7.83 (d, J = 8.4 Hz, 2H), 7.89 (d, J = 8.4 Hz, 2H), and 8.01 (d, J = 8.7 Hz, 2H). HRMS m/z $C_{14}H_{10}N_3OI$ found 362.9855/ calcd 362.9869 (M^+).

4.1.13. 4-(3-(4-Iodophenyl)-1,2,4-oxadiazol-5-yl)-*N*-methylaniline (13)

The same reaction as described above to prepare **12** was employed and 20 mg of **13** was obtained in a 86.0% yield from **8**. ^1H NMR (300 MHz, $CDCl_3$) δ 2.93 (s, 3H), 4.29 (s, 1H), 6.66 (d, J = 8.4 Hz, 2H), 7.85 (d, J = 8.4 Hz, 2H), 7.88 (d, J = 8.4 Hz, 2H), and 8.02 (d, J = 8.4 Hz, 2H). HRMS m/z $C_{15}H_{12}N_3OI$ found 377.0022/ calcd 377.0025 (M^+).

4.1.14. 4-(3-(4-Iodophenyl)-1,2,4-oxadiazol-5-yl)-*N*,*N*-dimethylaniline (14)

The same reaction as described above to prepare **12** was employed and 34 mg of **14** was obtained in a 72.4% yield from **9**. ^1H NMR (300 MHz, $CDCl_3$) δ 3.09 (s, 6H), 6.75 (d, J = 9.3 Hz, 2H), 7.83 (d, J = 8.7 Hz, 2H), 7.90 (d, J = 8.7 Hz, 2H), and 8.04 (d, J = 9.3 Hz, 2H). HRMS m/z $C_{16}H_{14}N_3OI$ found 391.0192/ calcd 391.0182 (M^+).

4.1.15. 3-(4-Iodophenyl)-5-(4-methoxyphenyl)-1,2,4-oxadiazole (15)

The same reaction as described above to prepare **12** was employed and 17 mg of **15** was obtained in a 69.2% yield from **10**. ^1H NMR (300 MHz, $CDCl_3$) δ 3.89 (s, 3H), 6.97 (d, J = 9.3 Hz, 2H), 7.48 (d, J = 8.4 Hz, 2H), 7.80 (d, J = 9.3 Hz, 2H), and 7.85 (d, J = 9.0 Hz, 2H). HRMS m/z $C_{15}H_{11}N_2O_2I$ found 377.9865/ calcd 377.9872 (M^+).

4.1.16. 4-(3-(4-Iodophenyl)-1,2,4-oxadiazol-5-yl)phenol (16)

The same reaction as described above to prepare **12** was employed and 14 mg of **16** was obtained in a 81.8% yield from **11**. ^1H NMR (300 MHz, $CDCl_3$) δ 6.99 (d, J = 8.7 Hz, 2H), 7.87 (d, J = 8.4 Hz, 2H), 7.88 (d, J = 8.1 Hz, 2H), and 8.12 (d, J = 8.1 Hz, 2H). HRMS m/z $C_{14}H_9N_2O_2I$ found 363.9704/ calcd 363.9709 (M^+).

4.2. Iododestannylation reaction

The radioiodinated forms of compounds **12**, **13**, **14**, and **15** were prepared from the corresponding tributyltin derivatives by iododestannylation. Briefly, to initiate the reaction, 50 μL of H_2O_2 (3%) was added to a mixture of a tributyltin derivative (100 μg/50 μL EtOH), [^{125}I]NaI (0.1–0.2 mCi, specific activity 2200 Ci/mmol), and 100 μL of 1 N HCl in a sealed vial. The reaction was allowed to proceed at room temperature for 10 min and terminated by addition of $NaHSO_3$. After neutralization with sodium bicarbonate and extraction with ethyl acetate, the extract was dried by passing it through an anhydrous Na_2SO_4 column and then blown dry with a stream of nitrogen gas. The radioiodinated ligand was purified by HPLC on a Cosmosil C18 column with an isocratic solvent of H_2O/acetonitrile (3/7) at a flow rate of 1.0 mL/min. The purified ligand was stored at −20 °C for the in vitro binding and biodistribution experiments.

4.3. Binding assays using the aggregated Aβ peptide in solution

A solid form of Aβ(1–42) was purchased from Peptide Institute (Osaka, Japan). Aggregation of peptides was carried out by gently dissolving the peptide (0.25 mg/mL) in a buffer solution (pH 7.4) containing 10 mM sodium phosphate and 1 mM EDTA. The solutions were incubated at 37 °C for 42 h with gentle and constant shaking. Binding experiments were carried out as described previously.[22] [^{125}I]IMPY (6-iodo-2-(4′-dimethylamino)phenyl-imidazo[1,2]pyridine) with 2200 Ci/mmol specific activity and greater than 95% radiochemical purity was prepared using the standard iododestannylation reaction as described previously.[13] Binding assays were carried out in 12 × 75 mm borosilicate glass tubes. The reaction mixture contained 50 μL of Aβ(1-42) aggregates (29 nM in the final assay mixture), 50 μL of [^{125}I]IMPY (0.02 nM diluted in 10% EtOH), 50 μL of inhibitor (8 pM-12.5 μM diluted in 10% EtOH), and 850 μL of 10% EtOH. Non-specific binding was defined in the presence of 400 nM IMPY in the same assay tubes. The mixture was incubated at 37 °C for 3 h and the bound and the free radioactivities were separated by vacuum filtration through Whatman GF/B filters using a Brandel M-24R cell harvester followed by 2 × 3 mL washes with 10% EtOH at room temperature. Filters containing the bound I-125 ligand were placed in a gamma counter (Aloka, ARC-380) for measuring radioactivity. Under the assay conditions, the specifically bound fraction accounted for less than 15% of the total radioactivity. Values for the half-maximal inhibitory concentration (IC_{50}) were determined from displacement curves using GraphPad Prism 4.0 (GraphPad Software, San Diego, CA), and those for the inhibition constant (K_i) were calculated using the Cheng-Prusoff equation.[23]

4.4. Neuropathological staining of model mouse brain sections

The Tg2576 transgenic mice (female, 23-month-old) were used as Alzheimer's model mice. After the mice were sacrificed by decapitation, the brains were immediately removed and frozen in powdered dry ice. The frozen blocks were sliced into serial sections, 10-μm thick. Each slide was incubated with a 50% ethanol solution (100 μM) of compound **14**. The sections were washed in 50% ethanol for 3 min two times. Fluorescent observation was performed with the Nikon system. Thereafter, the serial sections were also immunostained with DAB as a chromogen using monoclonal antibodies against β-amyloid (Amyloid β-Protein Immunohistostain kit, WAKO).

4.5. In vivo biodistribution in normal mice

The experiments with animals were conducted in accordance with our institutional guidelines and were approved by Nagasaki University Animal Care Committee. A saline solution (100 μL) containing ethanol (10 μL) of radiolabeled agents (0.5 μCi) was injected intravenously directly into the tail vein of ddY mice (5-week-old, 22–25 g). The mice were sacrificed at various time points post-injection. The organs of interest were removed and weighed, and the radioactivity was measured with an automatic gamma counter (Aloka, ARC-380).

Acknowledgments

This study was supported by the Program for Promotion of Fundamental Studies in Health Sciences of the National Institute of Biomedical Innovation (NIBIO) and Health Labour Sciences Research Grant.

References and notes

1. Selkoe, D. J. *Physiol. Rev.* **2001**, *81*, 741.
2. Hardy, J.; Selkoe, D. J. *Science* **2002**, *297*, 353.